ACS APPLIED MATERIALS & INTERFACES

Letter

www.acsami.org

CdS/CdSe Core–Shell Nanorod Arrays: Energy Level Alignment and Enhanced Photoelectrochemical Performance

Meng Wang, Jiangang Jiang, Jinwen Shi, and Liejin Guo*

International Research Centre for Renewable Energy & State Key Laboratory of Multiphase Flow in Power Engineering, Xi'an Jiaotong University, Shaanxi 710049, China

Supporting Information

ABSTRACT: Novel CdS/CdSe core–shell nanorod arrays were fabricated by a chemical bath deposition of CdSe on hydrothermally synthesized CdS nanorods. The CdS rods were hexagonal phase faced and the top of the rod was subulate. After the chemical bath deposition approach, CdS nanorod arrays were encapsulated by a uniform CdSe layer resulting enhanced absorbance and extended absorption edges of the films. A tandem structure of the energy bands of CdS/CdSe was also formed as a result of the Fermi level alignment, which is a benefit to the efficient separation of photogenerated charges. CdS/CdSe core–shell arrays gave a maximum photocurrent of 5.3 mA/cm^2, which was 4 and 11 times as large as bare CdS and CdSe, respectively.

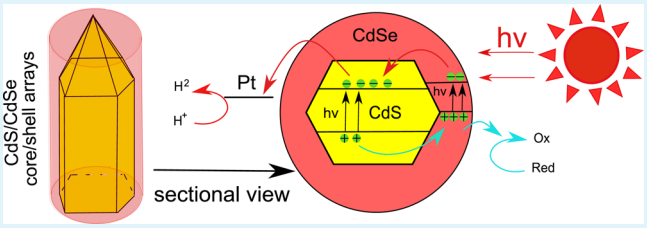

KEYWORDS: *core–shell, CdS, CdSe, Fermi level alignment, photoelectrochemistry*

Hydrogen production from water using powder catalysts or photocatalytic electrodes under the irradiation of sunlight has attracted extensive attention because of the energy dilemma and environmental contamination. Compared with nanoparticles, 1D geometry has a great deal of advantages such as enhanced solar light scattering and absorption ability, superior charge separation and transport properties, and other interesting structure dependent natures.[1] Among various 1D materials, quantum dots sensitized solar cells are promising photoelectrodes because of their excellent performance and low cost.[2] Metal oxide arrays are often used as the template to capture quantum dots. ZnO, TiO_2, and WO_3 with diverse micro/nanostructures like nanowires,[3−6] nanorods,[7−9] and nanotubes[10,11,30] are the most studied materials for the application of quantum dots sensitized solar cells. However, because the energy band gaps of metal oxides are always larger than 3.0 eV,[32] only ultraviolet light, which accounts for 4% in the solar spectrum, can be utilized. So the visible-light absorption efficiency of quantum-dot-sensitized metal oxide arrays was limited by the quality of the sensitizers.[12−14]

In this paper, core–shell CdSe/CdS nanorod arrays were achieved by a facile chemical bath deposition (CBD) approach to combine light absorption ability between CdS substrate and CdSe sensitizer. Solution chemistry synthesized CdS arrays were used as the template in the CBD process.[15] It is well known that, CdS has more negative conduction band (than the H_2O/H_2 redox potential) and higher charges separation efficiency.[16] Nevertheless, the energy band gap of CdS is 2.3 eV in bulk, which restricts its absorption edge below the wavelength of ca. 550 nm. Furthermore, CdS grown on the FTO substrate was extraordinary sparse and the length of them was approximate only 500−1000 nm, which limited the absorbance of CdS. CdSe quantum dots introduced as the sensitizer, can expand the absorption edge of the film from wavelength of ca. 550 nm (for CdS) to ca. 720 nm (for CdSe).[17] What's more, the CBD procedure could also increase the diameter of the rods, so the absorbance of the film was improved as well. To the best of our knowledge, CdSe-sensitized CdS nanorods with core–shell structure were synthesized by our group for the first time. Comparing with bare CdS and CdSe, the PEC performance of CdS/CdSe was significantly enhanced. Under the irradiation of 100 mW/cm^2, a photocurrent of 5.3 mA/cm^2 with applied potential of 0.7 V vs Ag/AgCl was achieved in this work.

CdS nanorod arrays were synthesized via a hydrothermal method similar to that described by Chen et al.[14] but with minor modification. The film was grown on fluorine-doped thin oxide (FTO) substrate. FTO coated glasses (TEC-15 15 Ω/sp) were cleaned by ultrasonic cleaning in acetone, deionized water and ethanol, and then dried under a stream of nitrogen. The thus-obtained FTO glass was put into a mixed aqueous solution of cadmium nitride $Cd(NO_3)_2{\cdot}4H_2O$ (0.0125 mol/L), thiourea (0.375 mol/L) and glutathione (0.0075 mol/L). Finally, the solution was maintained at 200 °C for 4 h followed by calcination at 400 °C for 30 min under a stable stream of nitrogen.

The depositing of CdSe quantum dots and the formation of core-shell CdSe sensitized CdS arrays were achieved by chemical bath deposition (CBD) approach. The Se source was from Na_2SeSO_3 which was prepared by dissolving 0.02 mol

Received: March 8, 2013
Accepted: April 22, 2013
Published: April 22, 2013

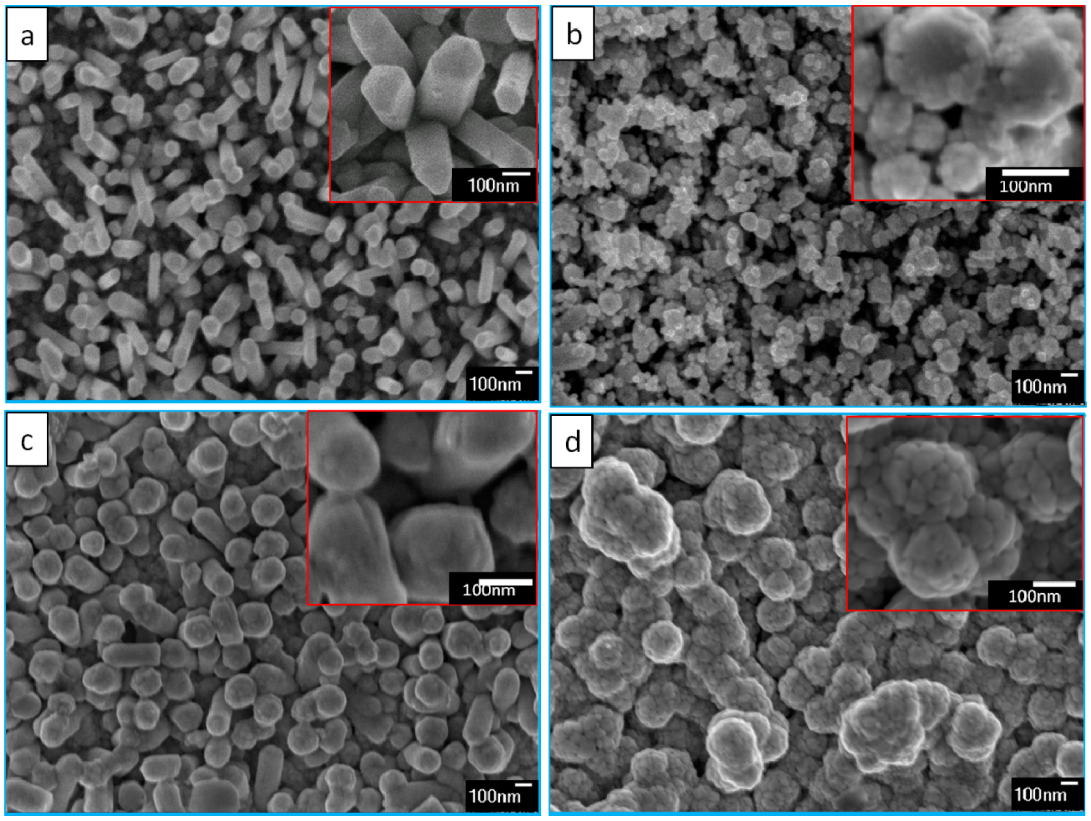

Figure 1. High-powered images of core shell CdSe/CdS and bare CdS arrays: (a) hydrothermal synthesized CdS; (b–d) CdSe/CdS after the treatment of CBD process, (b) 60 °C, 60 min;(c) 80 °C, 60 min; (d) 100 °C, 60 min.

of selenium powder into an aqueous solution (100 mL) of Na_2SO_3 (0.5 mol/L). Then the solution was maintained at 70 °C and refluxed for 5 h with a flow of nitrogen as the protection atmosphere. The thus-obtained Na_2SeSO_3 aqueous solution was stored at 60 °C in a conical beaker for further utilization. 0.505 g of KOH was added into 100ml of de-ionized water with magnetic stirring. Then nitrilotriacetic acid (0.57 g) was added into the solution after KOH was dissolved completely, followed by 30 minutes of stirring. Then 0.617 g of $Cd(NO_3)_2{\cdot}4H_2O$ was added into the solution with magnetic stirring for 5 min. The resulting transparent solution was maintained at the reaction temperature for 30 min, before CdS nanorod arrays was placed into the solution at a certain angle, 10 mL of Na_2SeSO_3 solution was added into the solution, which was maintained for different times. The samples were described as CdS/CdSe-A, where A represents the CBD temperature.

Figure 1a and Figure S5 in the Supporting Information show the SEM images of hydrothermal synthesized CdS nanorods. Uniform CdS rods coated on FTO substrate were exhibited, and the length of CdS nanorods was about 500–1000 nm. Figure S5b in the Supporting Information and the inset in Figure 1a show that the CdS rods were hexagonal phase faced and the top of the rod was subulate which is quite different with the result reported by Chen and co-workers.[15] The diameters of the rods were not uniform, distributing from 70 to 120 nm. After the deposition of CdSe, core shell structure was formed with CdS nanorods as the core and CdSe quantum dots as the shell. When the CBD temperature was at 60 °C, CdS could not be encapsulated by CdSe quantum dots uniformly (Figure 1b), some of them tended to aggregate to big clusters. As CBD temperature increased to 80 °C, CdSe was covered on CdS rods equably. The diameter of the rods was increased, and the rod got more compact (Figure 1c). If the CBD temperature was increased furthermore to 100 °C, CdSe quantum dots of the shell grew to bigger particles, and the rodlike structure of CdS became blurry (Figure 1d). XRD results are shown in Figure S1 in the Supporting Information. It shows that CdS rods were hexagonal phase faced (PDF card number: 01-075-1545). After the treatment with CBD approach, the intensity of CdS diffraction peaks (marked as *) decreased as the CBD temperature increased. Meanwhile, the diffraction peaks of CdSe (marked as #) became clearer. The XRD patterns confirmed well with the SEM images. The elemental EDX mapping of CdS/CdSe–80 was also measured as illustrated in Figure S2 in the Supporting Information. It shows that elements of S, Se, and Cd distributed homogeneously on the FTO substrate.

Panels a and b in Figure 2 show the transmission electron microscope (TEM) and high-resolution transmission electron microscopy (HRTEM) images of thus-obtained materials. CdS rods with smooth surface, and *d*-spacing fringes of 0.34 nm corresponding to (0002) lance plane of hexagonal CdS were observed (see Figure S2 in the Supporting Information). Furthermore, we can also see from the HRTEM images that the CdS was monocrystalline essentially and grew along the [001] direction, corresponding to the XRD results in Figure S1 in the Supporting Information. After the CBD approach, bare CdS rod was encapsulated with a layer of CdSe nanoparticles, and the thickness of CdSe shell distributed from 13.5 to 36.3 nm. *D*-spacing fringes of 0.37 nm matching (1010) planes of hexagonal CdSe and d-spacing fringes of 0.34 nm matching the (0002) lance planes of hexagonal CdS were also observed in

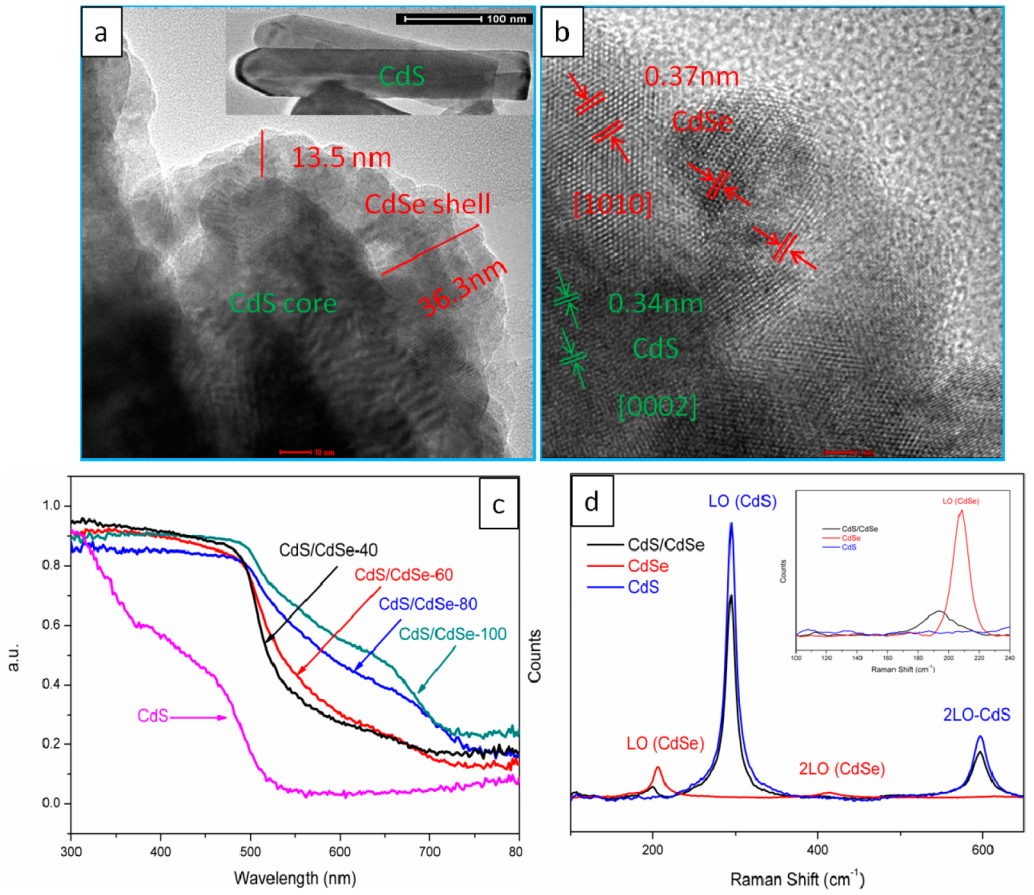

Figure 2. (a, b) TEM images and HRTEM images of bare CdS and core shell CdSe/CdS-80 rods respectively; (c) absorption spectra of bare CdS and core shell CdSe/CdS films; (d) Raman spectra of CdS, CdSe, and coreshell CdSe/CdS-80.

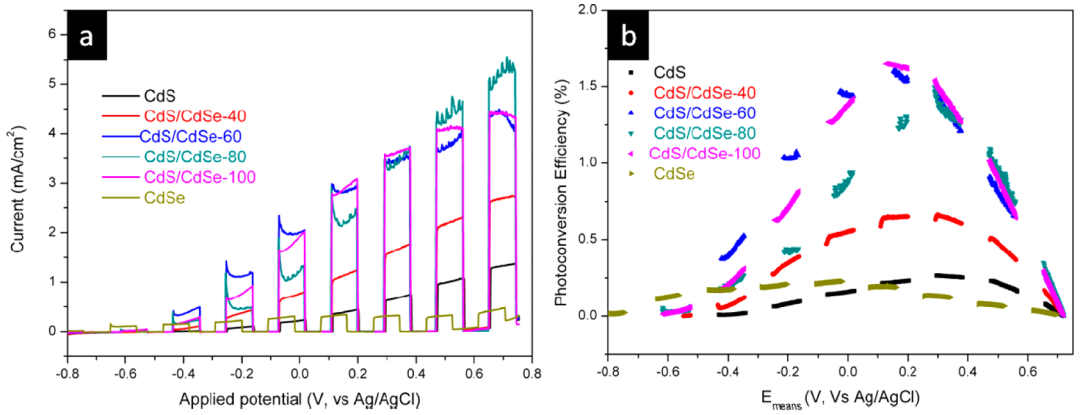

Figure 3. (a) Effect of CdSe deposition temperatures on the current−potential characteristics of as-prepared core shell CdSe/CdS films, and (b) photoconversion efficiency of as-prepared core shell CdSe/CdS films prepare at different CBD temperatures.

the HRTEM image (Figure 2b). As a result, the diameter of the rod was increased.

Light absorption activity of bare CdS and CdS/CdSe nanostructure arrays were investigated by UV − vis spectrometer (Figure 2c). The absorption edge of CdS appeared at about 520 nm. After the deposition of CdSe quantum dots, the absorption edges were expanded observably. Furthermore, as CBD temperature increased, the absorption edges gradually moved to infrared region (750 nm for CdS/CdSe−80). It is well-known that the absorption edges of CdSe quantum dots are markedly dependent on quantum size.[18,19] In this paper, CBD synthesized CdSe particle size grew significantly as the CBD temperature was raised (Figure 1c, d). So the absorption edges of core shell CdS/CdSe shifted to infrared region gradually. What's more, CdSe encapsulated CdS films exhibited higher absorbance in both UV region and visible region compared with bare CdS film. Figure 2c also shows an absorbance saltation of CdS/CdSe, which appeared around 520 nm, suggesting electrons and holes in CdS core can also be excited under the irradiation of sunlight. As is well-known, CdSe exhibits an enhanced light-harvesting effect. As the experimental temperature was raised, the amount of deposited

dx.doi.org/10.1021/am400851q | ACS Appl. Mater. Interfaces 2013, 5, 4021−4025

CdSe on CdS rods increased, which caused higher light absorbance for CdS/CdSe films.

As follows in Figure 2d, Raman spectra of core shell CdS/CdSe arrays, bare CdS, and bare CdSe films were investigated. Raman peaks of CdS related to the longitudinal optical (LO) phonon appeared at about 300 cm^{-1}, and its overtone (2 LO) appeared at about 600 cm^{-1}.[20] After the coating of CdSe shell, Raman peaks of CdSe related to the longitudinal optical (LO) phonon and its overtone (2 LO) also appeared which were at about 210 and 420 cm^{-1}, respectively.[21,22] Compared with pure CdSe film (red line in Figure 2d), Raman peaks at about 210 cm^{-1} (black line in Figure 2d) shifted to downward. Meanwhile, the Raman peak of CdS/CdSe at about 210 cm^{-1} became broader than that of CdSe. Both of these phenomena were due to the effect of phonons spatial confinement or the effect of the surface optical (SO) vibrations in small NCs (usually smaller than 10 nm), which were also observed in other reports.[23−25]

Influence of the CBD temperatures on the current−potential and photoconversion efficiency results of as-prepared core shell CdS/CdSe films are shown in Figure 3. Dark current density for all samples could be neglected, whereas upon irradiation, the photocurrent increased significantly. Meanwhile, all the CdSe-coated CdS electrodes existed enhanced current−potential performance as compared to bare CdS or CdSe films. A maximum photocurrent of 5.3 mA/cm^2 with applied potential of 0.7 V vs Ag/AgCl was achieved for core shell CdS/CdSe synthesized at CBD temperature of 80 °C. It was over 4 times and 11 times as large as bare CdS and CdSe films, respectively. Furthermore, the photoconversion efficiency of CdS/CdSe was also markedly improved from 0.23% (for bare CdS) to 1.6% (for CdS/CdSe).

The PEC stability of as-obtained CdS/CdSe arrays was investigated by the chronoamperometry (see Figure S6 in the Supporting Information), and 0.5 M of Na_2SO_3 electrolyte was utilized as a scavenger for an efficient hole scavenger for CdS and CdSe. Figure S6a in the Supporting Information shows the chronoamperometry of CdS/CdSe-80 versus different applied potentials. The photocurrent of CdS/CdSe steadily increased with applied potentials. Figure S6b in the Supporting Information shows long time chronoamperometry for CdS/CdSe-80 with an applied potential of 0 V vs Ag/AgCl. We can see that the photocurrent decreased continuously because of the hole-induced anodic corrosion of CdS and CdSe as the illumination time increased. The photocurrent decreased about 6% after 3600 s illumination. So the stability of this material should be improved furthermore for its future application. Recent decades, several methods (for example, using sulfide/polysulfide as the electrolyte,[31] purging the electrolytic cell with inert gas before the photocurrent measurement,[27] modifying with water-oxidation co-catalysts,[28,29] and coating with a passivated layer (such as ZnS) outside CdS or CdSe materials[26]) have been developed for this situation. Further studies to improve the stability of as-prepared CdS/CdSe core−shell arrays by the methods mentioned above are underway.

The high photocurrent performance of core−shell Cods/CdSe nanostructure arrays rely on the high separation efficiency of photogenerated charges. As shown in Figure 4, energy bands of CdS and CdSe are demonstrated. The Fermi levels for CdS and CdSe were −0.58 eV and −0.46 eV (vs Ag/AgCl) respectively.[26] When CdSe and CdS were brought in contact, electrons in CdS conduction band wound flow to CdSe, which

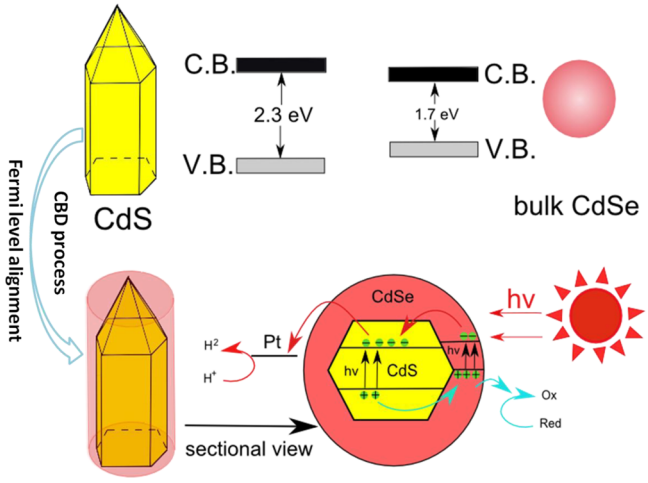

Figure 4. Relative band edges of CdS and CdSe in bulk phase and a stepwise band edge structure of CdSe/CdS for efficient separation and transport of photogenerated charges.

was caused by the difference of Fermi levels described above. This effect is known as Fermi level alignment. The redistribution of electrons caused band edge of CdSe upward shift and band edge of CdS downward shift. Furthermore, the resulting band edges of CdSe/CdS/FTO were forecasted to have a stepwise structure. The stepwise structure built in CdSe/CdS/FTO lead to not only the high electrons injection efficiency but also hole-recovery for both CdS core and CdSe shell. As a result, photocurrent performance and stability of the photoelectrode were both enhanced as shown in Figure 3 and Figure S6 in the Supporting Information.

In conclusion, core−shell arrays of CdSe/CdS nanorods were successfully synthesized through a facile CBD process using hydrothermal-prepared CdS nanorods as the template. SEM, TEM, and EDX mapping results revealed that CdS were encapsulated by a uniform CdSe layer, and the thickness of this layer could be effectively controlled by changing CBD temperature. Furthermore, CdSe layer coated on CdS markedly enhanced the visible-light absorption ability and photocurrent performance. Absorption edges of the films were extended from 525 to 750 nm and the photoconversion efficiency of core shell CdSe/CdS electrode was also improved from 0.23% (for bare CdS) to 1.6% (for CdSe/CdS). CdSe-sensitized CdS film with core−shell nanostructure was first synthesized by our group and this material should have enormous potential for various fields including catalysis, gas detection, electrochemistry, purification, and so on.

■ ASSOCIATED CONTENT

Supporting Information

Characterization details; photoelectrochemical measurement details; XRD patterns of bare CdS and core shell CdSe/CdS nanostructure arrays; SEM image and S, Se, and Cd elemental EDX mappings of core shell CdSe/CdS; TEM and HRTEM images of CdS rods; TEM and HRTEM images of CdS/CdSe core shell nanorod arrays; sectional view of CdS film; chronoamperometry with different applied potentials; and photocurrent versus time profiles. This material is available free of charge via the Internet at http://pubs.acs.org.

AUTHOR INFORMATION

Corresponding Author

*E-mail: lj-guo@mail.xjtu.edu.cn.

Notes

The authors declare no competing financial interest.

ACKNOWLEDGMENTS

This work was supported by the Natural Science Foundation of China (51121092 and 91010012), the National Basic Research Program of China NO. 2009CB220000).

REFERENCES

(1) Borchers, C.; Müller, S.; Stichtenoth, D.; Schwen, D.; Ronning, C. *J. Phys. Chem. B* **2006**, *110*, 1656−1660.
(2) Zhu, H.; Lian, T. *Energy Environ. Sci.* **2012**, *5*, 9406.
(3) Seol, M.; Ramasamy, E.; Lee, J.; Yong, K. *J. Phys. Chem. C* **2011**, *115*, 22018−22024.
(4) Lin, C.-J.; Chen, S.-y.; Liou, Y.-H. *Electrochem. Commun.* **2010**, *12*, 1513−1516.
(5) Sung, T. K.; Kang, J. H.; Jang, D. M.; Myung, Y.; Jung, G. B.; Kim, H. S.; Jung, C. S.; Cho, Y. J.; Park, J.; Lee, C.-L. *J. Mater. Chem.* **2011**, *21*, 4553.
(6) Jiao, Z.; Wang, J.; Ke, L.; Sun, X. W.; Demir, H. V. *ACS Appl. Mater. Interfaces* **2011**, *3*, 229−236.
(7) Wang, X.; Zhu, H.; Xu, Y.; Wang, H.; Tao, Y.; Hark, S.; Xiao, X.; Li, Q. *ACS Nano* **2010**, *4*, 3302−3308.
(8) Tang, Y.; Hu, X.; Chen, M.; Luo, L.; Li, B.; Zhang, L. *Electrochim. Acta* **2009**, *54*, 2742−2747.
(9) Chouhan, N.; Yeh, C. L.; Hu, S. F.; Huang, J. H.; Tsai, C. W.; Liu, R. S.; Chang, W. S.; Chen, K. H. *J. Electrochem. Soc.* **2010**, *157*, B1430.
(10) Lai, Y.; Lin, Z.; Zheng, D.; Chi, L.; Du, R.; Lin, C. *Electrochim. Acta* **2012**, *79*, 175−181.
(11) Gao, X.-F.; Li, H.-B.; Sun, W.-T.; Chen, Q.; Tang, F.-Q.; Peng, L.-M. *J. Phys. Chem. C* **2009**, *113*, 7531−7535.
(12) Owens, S. A.; Carpenter, M. C.; Sonne, J. W. H.; Miller, C. A.; Renehan, J. R.; Odonkor, C. A.; Henry, E. M.; Miles, D. T. *J. Phys. Chem. C* **2011**, *115*, 18952−18957.
(13) Robel, I.; Subramanian, V.; Kuno, M.; Kamat, P. V. *J. Am. Chem. Soc.* **2006**, *128*, 2385−2393.
(14) Ma, W.; Luther, J. M.; Zheng, H.; Wu, Y.; Alivisatos, A. P. *Nano Lett.* **2009**, *9*, 1699−1703.
(15) Chen, F.; Zhou, R.; Yang, L.; Shi, M.; Wu, G.; Wang, M.; Chen, H. *J. Phys. Chem. C* **2008**, *112*, 13457−13462.
(16) Matsumura, M.; Saho, Y.; Tsubomura, H. *J. Phys. Chem.* **1983**, *87*, 3807−3808.
(17) Kim, H.-S.; Ko, S.-B.; Jang, I.-H.; Park, N.-G. *Bull. Korean Chem. Soc.* **2011**, *47*, 12637.
(18) Regulacio, M. D.; Han, M.-Y. *Acc. Chem. Res.* **2010**, *43*, 621−630.
(19) Nam, D.-E.; Song, W.-S.; Yang, H. *J. Mater. Chem.* **2011**, *21*, 18220.
(20) Jing, D.; Guo, L. *J. Phys. Chem. B* **2006**, *110*, 11139−11145.
(21) Dzhagan, V. M.; Valakh, M. Y.; Raevskaya, A. E.; Stroyuk, A. L.; Kuchmiy, S. Y.; Zahn, D. R. T. *Nanotechnology* **2007**, *18*, 285701.
(22) Nesheva, D.; Raptis, C.; Levi, Z. *Phys. Rev. B* **1998**, *58*, 7913−7920.
(23) Hwang, Y.-N.; Shin, S.; Park, H. L.; Park, S.-H.; Kim, U.; Jeong, H. S.; Shin, E.-j.; Kim, D. *Phys. Rev. B* **1996**, *54*, 15120−15124.
(24) Campbell, I. H.; Fauchet, P. M. *Solid State Commun.* **1986**, *58*, 739−741.
(25) Zhang, W.; He, Y.; Zhang, M. *J. Phys. D* **2000**, *33*, 912−916.
(26) Lee, Y.-L.; Chi, C.-F.; Liau, S.-Y. *Chem. Mater.* **2010**, *22*, 922−927.
(27) Hou, D.; Dev, A.; Frank, K.; Rosenauer, A.; Voss, T. *The J. Phys. Chem. C* **2012**, *116*, 19604−19610.
(28) Seol, M.; Jang, J.-W.; Cho, S.; Lee, J. S.; Yong, K. *Chem. Mater.* **2013**, *25*, 184−189.
(29) Chen, H. M.; Chen, C. K.; Chen, C.-J.; Cheng, L.-C.; Wu, P. C.; Cheng, B. H.; Ho, Y. Z.; Tseng, M. L.; Hsu, Y.-Y.; Chan, T.-S.; Lee, J.-F.; Liu, R.-S.; Tsai, D. P. *ACS Nano* **2012**, *6*, 7362−7372.
(30) Wang, M.; Jiang, J.; Liu, G.; Shi, J.; Guo, L. *Appl. Catal., B: Environ.* **2013**, *138-139*, 304−310.
(31) Lee, Y.-L.; Chang, C.-H. *J. Power Sources* **2008**, *185*, 584−588.
(32) Shi, J.; Guo, L. *Prog. Nat. Sci: Mater. Int.* **2012**, *22*, 592−615.